Enhancement of synthetic jets by means of an integrated valve-less pump

Part II. Numerical and experimental studies

Zdeněk Trávníček[a], Václav Tesař[b] and An-Bang Wang[c]

[a]Institute of Thermomechanics, Academy of Sciences of the Czech Republic, Dolejškova 5, 182 00 Prague 8, Czech Republic
[b]The University of Sheffield, Mappin Street, Sheffield S1 3JD, UK
[c]National Taiwan University, Institute of Applied Mechanics, 1 Roosevelt Road, Sec. IV, 106 Taipei, Taiwan, ROC

Received 16 June 2004; revised 7 December 2004; accepted 31 March 2005. Available online 25 May 2005.

Abstract

The paper studies the performance of the new fluid jet actuator based on the novel principle of the generation of fluid jet, which has been presented in [Z. Trávníček, A.I. Fedorchenko, A.-B. Wang, Enhancement of synthetic jets by means of an integrated valve-less fluid pump. Part I. Design of the actuator, Sens. Actuators A, 120 (2005) 232–240]. The fluid jet actuator consists of a synthetic jet actuator and a valve-less pump. The resulting periodical fluid jet is intrinsically non-zero-net-mass-flux, in contrast to the traditional synthetic jet. The numerical results have been compared with the laboratory experiments comprising phase-locked smoke visualization and time-mean velocity measurements. The results have confirmed the satisfactory performance of the actuator.

Keywords: Actuators; Synthetic jet; Coaxial jet; Valve-less pump; Visualization; Numerical simulation

Article Outline

1. Introduction

Actuators based on the synthetic jet idea became recently of increasing importance for a number of applications. The interest was triggered mainly by publications of Glezer et al., the first of which was the Patent [2].

The name “synthetic jets” was derived from the idea of their being produced or synthesized from the train of individual vortical structures (often of the character of vortex rings) generated by periodic alternating flows into and out from a nozzle. This inflow and outflow is produced by periodic alternating displacement and ingestion of fluid from and into the nozzle. In a typical layout, a sealed displacement cavity is provided with the nozzle at its one end and an actuating piston or diaphragm at the other end, the periodic movements of which result in periodic variations of the available volume inside the cavity. There is no time-mean mass flux of fluid into the cavity and hence also through the nozzle. This is why another common description of the generated flowfield is zero-net-mass-flux jet. The positive jet-like flow away from the nozzle is generated due to the non-linearity of the governing hydrodynamic equations, which makes the ingestion part of the flow cycle different from the outflow part. The time-mean mass flow rate is, of course, zero only in the nozzle exit cross section. With progressing distance from the nozzle the time-mean mass flux increases in a similar manner as in standard steady jets. The difference between the inflow and outflow phases (the outflow reaching farther because of the inertia gained inside the nozzle) may be described as a form of rectification and in fact it is related to the rectification phenomena used in fluidic pumping where it is used to replace the conventional suction and displacement one-way valves.

The rectification principle was investigated earlier and some important facts were published already in 1980s [3] and [4]. The current interest, however, was aroused by [2] and [5] in 1998, which also introduced the new name (“synthetic jet”) presently used to describe the phenomenon. Soon thereafter, basic forms of synthetic jets were investigated by several authors, e.g. [6], [7], [8], [9], [10], [11], [12], [13] and [14], mainly with view of the prospective applications in jet vectoring [10], active control of turbulence or flow separation both in external [11], [12] and [13] as well as internal aerodynamics [14].

Another very promising field is high-intensity heat/mass transfer, typically for cooling applications. The first publication about this field in a reviewed journal was published by Trávníček and Tesař [15], although the idea had appeared before (e.g. [2], [16] and [17]). The layouts considered are similar to the well-known impinging jets: the jet generating nozzle is directed towards the cooled surface. The advantage of the synthetic jets is the simplicity of the cooling systems, which need neither blower nor distribution piping, otherwise occupying an overwhelming proportion of the system volume, in some cases (cooling of microprocessors) even larger volume than those of the actual microprocessors themselves.

Practically all the above-mentioned synthetic jets applications may be applied in devices of macro- as well as micro-size. In fact, in the microscale or microelectromechanical systems (MEMS) many advantages become more pronounced because of the basic physical principles: scaling down is usually associated with decreasing Reynolds numbers, which complicates mixing as well as convective heat transfer, typically poor in the laminar flow regime. It should be noted that typical development strategy followed by many researchers begins at macro-size and scaled-up laboratory models, the subsequent step (which, of course, may lead to practical micro-fabrication problems and crucial difficulties of operation at small Reynolds numbers) being the scaling down to the final micro-size. Characteristically, early investigations of synthetic jet used macro-size actuators [5], [6], [7], [8], [9], [10], [11], [12], [13], [14], [15], [16] and [17], and only recently micro-fabrication in silicon was used by Mallinson et al. [18].

2. The new hybrid principle

A fluidic pump driven by alternating air flow was developed by one of the present authors [3] for an application in nuclear fuel re-processing. The efficiency of the rectification of the driving alternating flow was investigated in [4]. Other principles of such non-moving-part fluidic pumping systems are described, e.g. in [19] and [20]. Recently, of particular interest became a version of a fluidic pump using the *rectification properties of diffusers*, [21], [22], [23], [24] and [25]. The advantage of this simple rectifying element, substituting the suction valve of traditional piston pumps, is the ease of fabrication especially at microscale.

Recently, the novel method of fluid jet generation and the novel fluid flow actuator have been proposed by Trávníček et al. [1] and [26]. The periodic fluid jet, which is called the "*double acting synthetic jet*" (D-SyJ), is intrinsically a non-zero-net-mass-flux jet even at the nozzle exit level. Similarly, as in pure synthetic jets, the resultant D-SyJ is generated mainly from a train of individual vortical "puffs", however, it is also partly produced by means of non-zero-net-mass-flux pumping function of the actuator (thus the "*Hybrid Jet*" name was suggested in [26]). Therefore, the volume flow rate as well as fluid momentum can be higher in comparison with a pure (zero-net-mass-flux) synthetic jet and this is another advantage, which may lead to useful applications.

The present paper describes a continuation of the previous work [1], in which the D-SyJ actuator has been proposed, and the prototype has been experimentally tested. A further development of the actuator as well as better understanding of fluid mechanics of the D-SyJ requires a wide and systematic approach, and this is the primary task of the present paper. Particularly efficient for such a goal is a combination of experimental and numerical investigations. The present paper describes an initial step of these combined investigations. Similarly as in [1], the study has been made with a macro-sized prototype.

3. The prototype of the D-SyJ actuator and used experimental methods

Fig. 1 shows a schematic view on the used D-SyJ actuator, corresponding to the description in [1], where a more detailed discussion of the actuating principle and of the experimental set-up is described. The actuator geometry is coaxial: The actuator consists of two distinguishable parts (or partial actuators), namely F (front) chamber that produces the central SyJ and R (rear) chamber that generates the annular jet. The chamber 1 and the inner nozzle supports 5 fix entire actuator together. The diaphragm 2a of the loudspeaker 2b is the common interface for both chambers F and R. The SyJ is generated from chamber F through its circular nozzle (or output element, 3a) as with other SyJ actuators such as the actuator described in [5]. On the other hand, the annular jet is generated from R chamber, which is consisted of annular nozzle 3b and conical ducts 4 as output and input elements, respectively. Input elements consist of 12 identical radial conical ducts (4), equidistantly located on the chamber 1. The actuator operates in double acting regime, i.e., both the up as well as the down-strokes of the diaphragm act on the displaced fluid: A positive, upwards stroke pushes fluid through the central circular nozzle, while the reverse down-stroke pushes fluid through the annular nozzle. The central circular jet is therefore the standard zero-net-mass-flux synthetic jet [5]. On the other hand, the annular jet is a non-zero-net-mass-flux jet. The axisymmetric coordinate system (x, r) is also shown in Fig. 1.

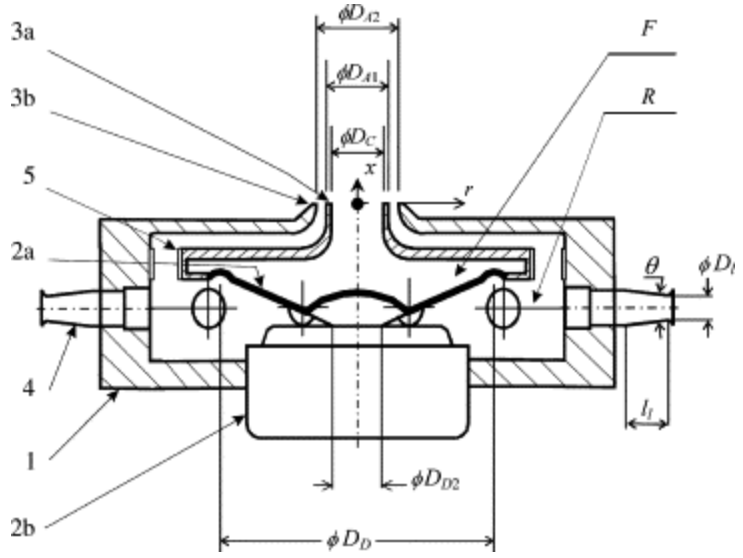

Fig. 1. Investigated coaxial double acting actuator, [1]. F, front cavity; R, rear cavity; 1, chamber; 2a, loudspeaker diaphragm; 2b, loudspeaker coil; 3a, central circular (output) nozzle; 3b, annular (output) nozzle; 4, input elements, namely 12 conical ducts; 5, inner nozzle supports; $ØD_{A2}$ = 16.6 mm, $ØD_{A1}$ = 12.0 mm, $ØD_C$ = 10.6 mm, $ØD_D$ = 53.0 mm, $ØD_{D2}$ = 9.0 mm, $ØD_l$ = 4.35 mm, l_l = 8.0 mm, θ = 12.5°.

The operating fluid in the present case is atmospheric air. It is driven by the loudspeaker of 66.5 mm diameter (MONACOR SP-7/4S, nominal electrical parameters 4 Ω, 4 W-rms, 8 W-max). The loudspeaker diaphragm is shaped as a cone, relatively rigid, covered by a spherical cap in the central part. The diaphragm is axially driven by the loudspeaker coil in the central part of diameter D_{D2} = 9 mm, and fixed on the loudspeaker chassis through a very flexible rim of middle diameter D_D = 53 mm. Because of this construction, it is quite plausible to consider the air as being driven by a rigid double-acting piston of diameters D_D/D_{D2} (it is quite different situation from planar flexible membranes, which are frequently used, e.g. by Smith and Glezer [5]).

The actuator loudspeaker was driven by the sinusoidal current from the sweep/function generator (THURLBY-THANDAR TG230), amplified by an in-house built power amplifier. The true rms a.c. current and voltage have been measured by a pair of digital multimeters (HP3478A) with the accuracy ± 1.5 and ± 0.46%, respectively. All experiments described in the present paper were performed with identical electric input power fed to the loudspeaker, 2.0 W (computed as a product of current and voltage).

The experimental step was mainly used for phase-locked flow visualization, which has been made by a multi-smoke wire technique: the flowfield was illuminated by a flashlight, and the in-house built electrical circuit was used for phase-locked synchronization of the sequence of three steps: camera shutter release, delayed smoke-wire heating with smoke generation, and flashlight initiation after the other delay. The accuracy of both delays was of the order of 10 μs, which was sufficient to match taking picture with an arbitrary moment of the driven cycle. Contrasting white streaklines on black background were observed and photographed by a digital camera (NICON CoolPix 990).

The time-mean velocity profiles were measured by the thermal velocity sensors (TESTO 490, a spherical sensor Ø2.5 mm, accuracy 5%, see [1]). The probe was positioned manually by 3-axis positioning system with the resolution 0.01 and 0.02 mm in radial and axial direction, respectively. Two K-thermocouples were used to measure air temperature; one was inserted into the cavity of the actuator while the other measured the ambient temperature. Maximal difference between the temperature of air inside the cavity and the ambient (due to the dissipation of incoming power) was 2 K for all experiments in this paper.

4. Numerical flowfield computations

The processes taking place in the new configuration of the actuator as well as in the generated jet were investigated by numerical computations of the flowfield. The computations were performed using the commercially available finite-volume CFD software package FLUENT 5 [27]. The fluid flow was assumed to be incompressible, isothermal, and turbulent. The fluid properties (density and viscosity) were inserted as constant. The unsteady version of the CFD package was used, permitting detailed investigations of the flowfield at 24 individual instants of the operation cycle. The

governing equations were solved for continuity, time-averaged momentum components in all three directions, turbulent kinetic energy, and turbulent energy dissipation rate.

The computations used an implicit formulation and worked with absolute (i.e., not dimensionless) values of the variables. Continuity and momentum equation were coupled by the SIMPLE algorithm, which works in predictor–corrector steps. Standard scheme provided as default by the software was used for the pressure evaluation and also standard default first-order upwind scheme was used in the momentum, turbulent kinetic energy, and turbulent energy dissipation rate equations. The multi-grid method to accelerate the convergence, and iterative technique with under-relaxation predictions of the velocity and pressure were used. Default under-relaxation factors of the solver were used, the values of which were 0.3, 0.7, 0.8 and 0.8 for the pressure, momentum, turbulent kinetic energy, and turbulent energy dissipation, respectively [27]. At each time step, the iterations proceeded up to the stage at which the convergence criteria for the residua were met. The solution was considered to be converged when the all values of the normalized residuals were less then 10^{-3}. This value, less than recommended for time-dependent solutions by the software provider [27], was found in previous computations of analogous problems [9] to be the best compromise between the solution accuracy and solution duration. The computations were performed using the Sheffield University "Titania" High Performance Computer Grid. Typical computation run for each of the 24 time steps computed in each oscillation cycle usually took less then a half-an-hour to converge. Most demanding for available computational resources was the large number of oscillation cycles, typically 50 but in some cases more than 100 that had to be computed before oscillation cycle became sufficiently indistinguishable from a previous one. This identity of cycles corresponds to damping out of the influence of the initial conditions and attaining the "quasi-steady" regime. The cycle-to-cycle deviations considered sufficiently small for progressing to the next computation were approximately less than 3% of the amplitude. No numerical criterion was applied, however, since the variations between subsequent cycles were generally not of the same character under different conditions; the identity of cycles was judged visually from plotted cycle histories.

4.1. Turbulence model and the present near-wall modelling

The model of turbulence used the scalar turbulent viscosity concept and as such was unable to resolve anisotropy. In particular, the model used was the renormalization group (RNG) k–ε turbulence model [27], which was found to yield reasonable results in similar computation problems [9] and in comparison with more complex models requires much shorter computing time. Near-wall modelling was based on the standard wall functions. The default set of the constants of the turbulence model was used, as provided by the software supplier [27]: $C_\mu = 0.0845$, $C_{1\varepsilon} = 1.42$, $C_{2\varepsilon} = 1.68$, $\beta = 0.012$ and $\eta_0 = 4.38$.

4.2. The domain, grid, boundary conditions and input data

Fig. 2 gives some idea about the computational domain and the unstructured grid used. The domain was a three-dimensional 30° sector bounded by two symmetry planes, one passing through the axis of the input element and the other halving the angle between the element axes (real 3D situation with 12 input elements was simulated to be periodical around the perimeter). Fig. 2(a) shows the grid in one of the bounding symmetry planes. The geometry of the computational domain corresponds to that of the experimental model (Fig. 1), with added hemispherical volumes upstream from the diffuser, denoted as position 6 in Fig. 2(b). Also, a large cylindrical volume (denoted as position 7 in Fig. 2(b)) was added downstream from the nozzles, representing the part of the atmosphere in which the generated jet is formed. The unstructured triangular grid was adapted in the course of the computations by dividing into smaller cells those finite volumes in which there was exceptionally high velocity magnitude gradient. Fig. 2(c) present several sections through the grid. As initially produced by GAMBIT pre-processing software, the grid possessed 43, 423 finite volumes. After the gradual refinements (performed in several steps, the first one by delimiting two spherical refinement regions geometrically, the following steps concentrating on the regions of the highest velocity magnitude gradients) the final grid used in most computation runs consisted of 80,012 tetrahedral cells, with 171,524 faces and 19,490 nodes.

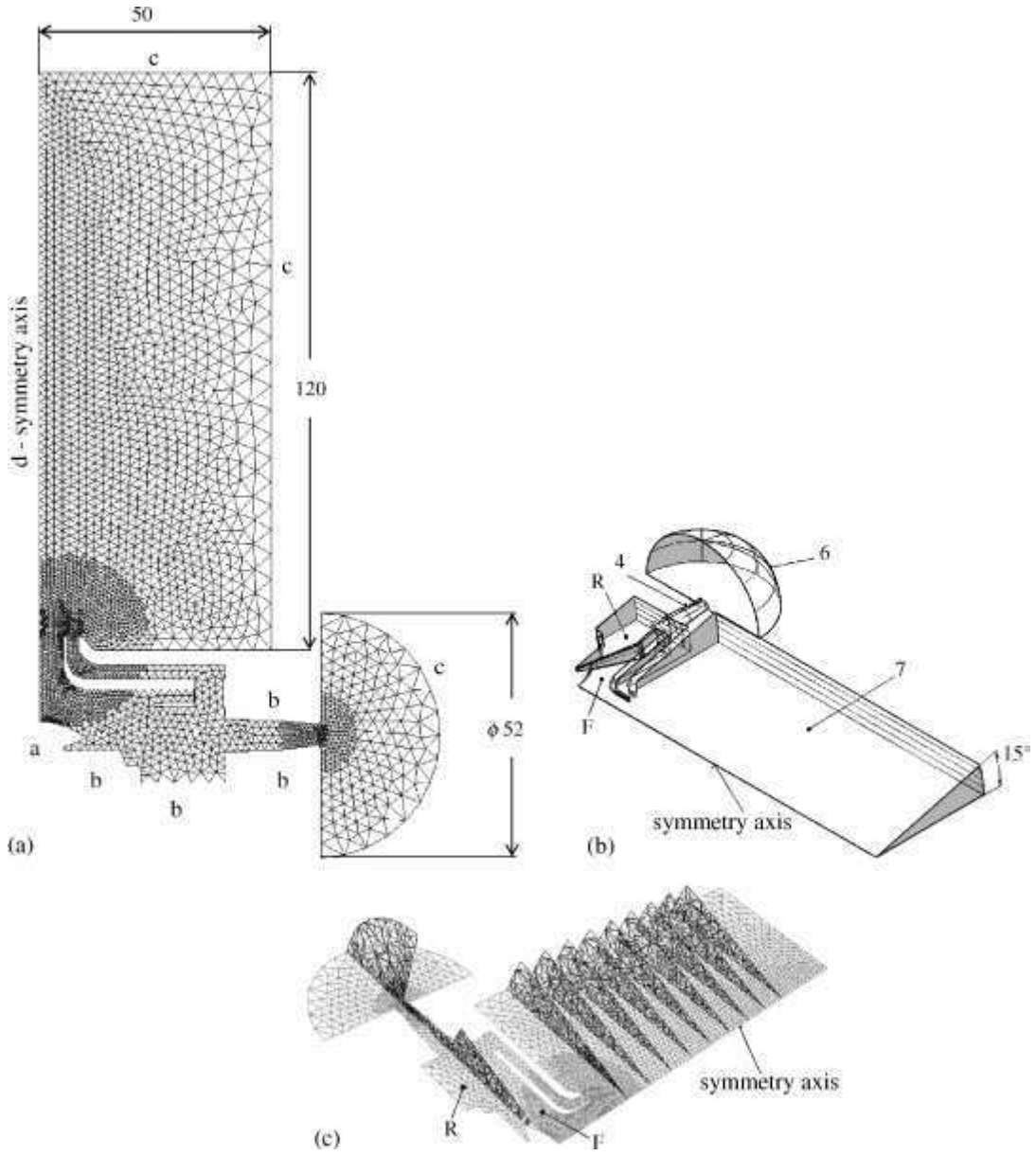

Fig. 2. Computational domain and the unstructured grid; (a) view of the symmetry plane with the prescribed boundary conditions a–d, (b) three-dimensional computational sector, (c) grid in the sector. F, front cavity; R, rear cavity; 4, input elements; 6, additional hemispherical volume; 7, cylindrical downstream volume.

The prescribed boundary conditions chosen for the computations were as follows, see Fig. 2:

(a) Driving diaphragm: Because of the reasonably rigid diaphragm, it was represented to be a double-acting shaped piston of diameters D_D and D_{D2} (see Fig. 1) with

a harmonic movement $x = x_{max}\sin(2\pi ft)$, where x_{max} is maximum diaphragm displacement from its neutral position, f is frequency and t is time. It should be noted that the period origin is defined at the neutral position of the diaphragm. This means that the central nozzle at this instant is in the displacement stroke while the annular jet is in antiphase, ingestion stroke, see [1]. The boundary condition is prescribed in form of axial velocity on the diaphragm surface $U = U_{max}\cos(2\pi ft)$, where $U_{max} = 2\pi f x_{max}$. Understandably, from the point of view of the both front/rear diaphragm surfaces, the velocity U represents a fluid source/sink in the same instant. The prescribed values of f and U_{max} agree with the "nominal operating point" of the D-SyJ actuator prototype, which has been defined in [1] at $f = 90$ Hz and $x_{max} = 1.5$ mm, therefore $U_{max} = 0.848$ m/s. The radial velocity component is prescribed zero on the diaphragm surfaces.

(b) Actuator fixed walls: A no-slip boundary condition, i.e., all velocity components are zero.

(c) Outlet: A static pressure was prescribed as reference value, 98,000 Pa. It allows a recirculation flow, i.e., fluid can enter the domain.

(d) Nozzle axis: The symmetry axis of the domain, representing the intersection of the two bounding symmetry planes set at 30°.

Fluid properties of working fluid (air): fluid density, $\rho = 1.225$ kg/m^3; dynamic viscosity, $\mu = 1.7894 \times 10^{-5}$ kg/(ms).

5. Results and discussions

The results of the flow visualization are compared with the numerical simulations in the sequence of photographs in Fig. 3 in the left and right columns of images, respectively. The photographs were taken phase-locked to the actuating signal at six equal time intervals during the actuating period. For better illustration, the time period of actuation signal has been chosen to be represented by 360 angular degrees. Therefore, the angle φ (from 0 to 360°) is used as the measure of the dimensionless time in a cycle t/T, where T is the period ($T = 1/f$). The numerical solutions in the right column of Fig. 3 also show phase-locked pathlines inside the actuator where the visualization experiments could not be performed.

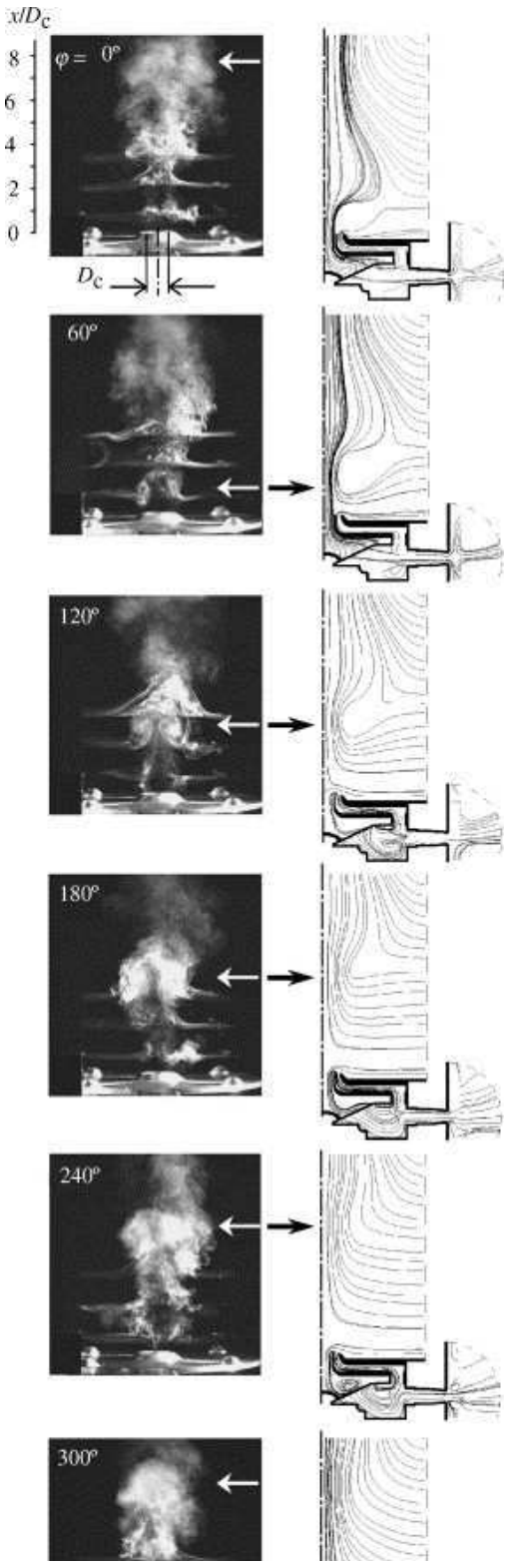
x/Dc
8
6
4
2
0
φ = 0°
Dc
60°
120°
180°
240°
300°

Fig. 3. Phase-locked smoke visualization compared with numerical simulations.

The main feature, visible in the sequence of photographs in Fig. 3, is the generated fluid "puff", i.e., the large vortex structure passing through the observation area. A location of the structure is indicated by the white arrow in the photographs. Of course, successive images do not show the same structure; the visualization sequence has been taken during a few minutes of a well stabilized regime of the jet actuation.

An extrusion of fluid through the central nozzle, and formation of the large vortex structure near the nozzle is very well visualized at $\varphi = 60$ to 120° when the central synthetic jet is in the outflow stroke. At the same time, fluid is ingested by the outer annular nozzle. The main proportion of this fluid comes from the relatively quiescent surroundings, and only a small portion is taken from just extruded central puff.

Later, at $\varphi = 120$ to 360°, the dominant large vortical structure is seen to move downstream. The development and later breakdown cause the boundary of the structure, which is originally quite clear at $\varphi = 60$ and 120°, to become blurred and finally almost indistinguishable at the end of cycle (see $\varphi = 300$ and $\varphi = 0°$ which corresponds to 360°).

It should be noted that the central nozzle operates in the inflow stroke at $\varphi = 120$, 180 and 240°, ingesting the external fluid. This is well visualized in the frame taken at $\varphi = 240°$. However, the inertia of the large vortex structure results in its moving downstream independently of the local situation in the nozzle, where flow orientation is reversed. At the same time, the annular nozzle pushes fluid outwards from the actuator. However, this annular D-SyJ outflow is practically invisible in the present photographs, because a large portion of the annular puff reverses inwards into the central nozzle very soon after having left the annular exit. Obviously, the central nozzle has no other possibility from where to suck fluid except from the surrounding annular jet.

Finally, at $\varphi = 300$ to 360°, the next outflow stroke from the central nozzle takes place and the next fluid puff from the central nozzle starts to be generated. The whole cycle is then repeated.

The right column of Fig. 3 shows pathlines obtained from the numerical computations at the same φ. There is a qualitative agreement between experiments and numerical simulation, which seems to be quite satisfactory: The position of the white arrow, which shows passing of the large vortex structure downstream frame by frame in the experiment, agrees well with maximum turning of the computed pathlines of the entrained fluid. The agreement is apparent particularly at $\varphi = 60$ to 240° as indicated by the black arrows in Fig. 3.

The position of the large vortex structure in the photographs in Fig. 3 was plotted in Fig. 4, which thus presents the relationship between the distance of this structure from the nozzle (dimensionless as x_v/D_C) versus φ. The diagram shows the celerity or propagation velocity [5] of subsequent individual fluid structures. Locations of two

structures are plotted in the graph: at the beginning of the investigated cycle (φ = 0 to 30°), one large structure is located rather far from the nozzle (x_v/D_C = 7.8–8.2), and it breaks down more downstream for x_v/D_C > 8.2. The subsequent structure is visualized during the rest of the cycle, see Fig. 4 at φ = 60 to 360° and the white arrows in Fig. 3 at φ = 60 to 300°.

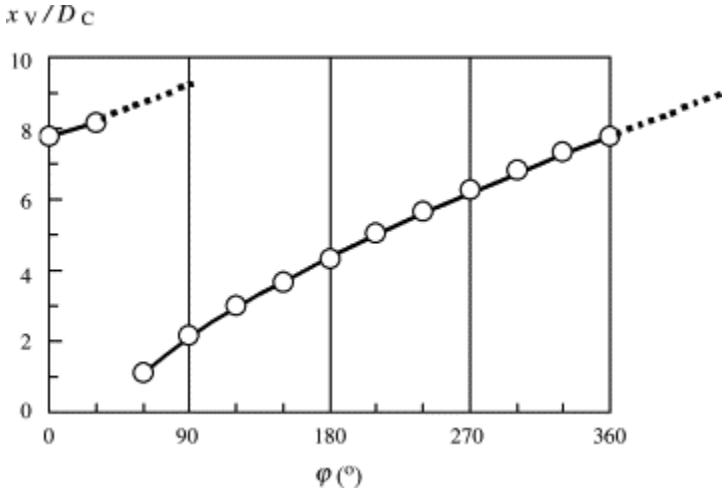

Fig. 4. Propagation of the large vortex structure during one cycle; evaluated from the visualization experiments.

It is worth noting that the smoothness of the graph in Fig. 4 indicates the reliability of the present phase-locked visualization. Moreover, Fig. 4 can be interpreted from a point of view of the "slug" flow model, i.e., a piston flow with identical velocities in the entire cross section, when the "pump stroke length" [1] (another term introduced by Tesař [9] is the "equivalent extruded column length") is defined for the central circular synthetic jet as $L_{OC} = V_{OC}/A_{OC}$, where V_{OC} is fluid volume extruded during pump stroke through the nozzle, and A_{OC} is the nozzle cross section area. The pump stroke of the central jet occurs from φ = 270° through 360 to 90° (it is broken by the period origin φ = 0°). A related motion of the large fluid structure is seen during this stroke from x_V/D_C = 6.2 through 7.8 to approximately 9.0 (the last value is an extrapolation beyond the structure breakdown, as shown by dotted lines in Fig. 4). The corresponding shift of the fluid structure (during the pump stroke) is $\Delta x_V/D_C$ = 9.0–6.2 = 2.8. Obviously, celerity of the fluid structure is higher near the nozzle, and it decreases farther away from the nozzle. For example, the fluid structure moves for φ = 60 to 90° from its location at x_V/D_C = 1.1–2.2. The equivalent shift of the fluid structure during the whole pump stroke (one-half of cycle) could be $\Delta x_V/D_C$ = 6 × (2.2–1.1) = approximately 6. It can be expected that both values of $\Delta x_V/D_C$ = 6 and 2.8 should agree with higher and lower limit of the "pump stroke length": the former value is related to the near nozzle (initial) region, the latter value to the structure breakdown area further downstream, respectively. In fact, as may be seen in Table 2 of paper [1], the "pump stroke length" is L_{OC} = 37.2 mm thus L_{OC}/D_C = 3.50. This value satisfactorily matches both limits.

Fig. 5 presents the variation of velocities during the actuator operating cycle obtained by evaluating the numerical solution. The computed axial velocity distributions along the jet centerline (x is the longitudinal coordinate, see Fig. 1) are plotted at different time instants (which are represented by $\varphi = 0$ to 360°). During the actuating cycle, the fluid "puff" goes downstream and the diagram shows the corresponding movement of the velocity maximum. The highest instantaneous velocity of fluid issuing from the central circular nozzle, 22.3 m/s, is seen to occur at $\varphi = 0°$, when the actuating diaphragm passes through its neutral position. This logical result, of course, agrees well with the continuity condition.

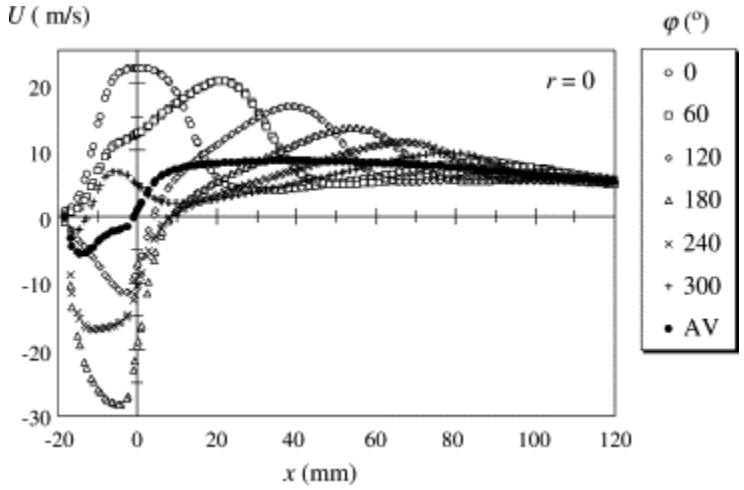

Fig. 5. Computed centerline velocity in the generated jet during one cycle; AV, the time-mean velocity.

The time-mean velocity along the centerline is plotted in Fig. 5 as well (the solid symbols); it was calculated as the average of all 24 instantaneous velocity distributions. Its maximum time-mean value 8.4 m/s was found at $x = 39.6$ mm. Further downstream, the computations show only very small velocity decrease, which is somewhat non-realistic (it will be discussed at Fig. 7 below). Moreover, Fig. 5 shows clearly that the axial velocity changes its sign up only to the distance $x < 9.1$ mm (i.e., $x/D_C < 0.86$) from the nozzle. This is "the range of actuator suction"; further downstream only positive velocities exist on the centerline during the whole cycle.

Fig. 6 shows centerline velocities during the actuating cycle, namely velocity oscillations at the indicated five points ranging from $x = 20$ to 80 mm (x is the longitudinal coordinate, see Fig. 1). The diagram demonstrates the development of the cycle shape, phase shift of velocity amplitude downstream, and gradual diminishing of velocity oscillations with axial distance.

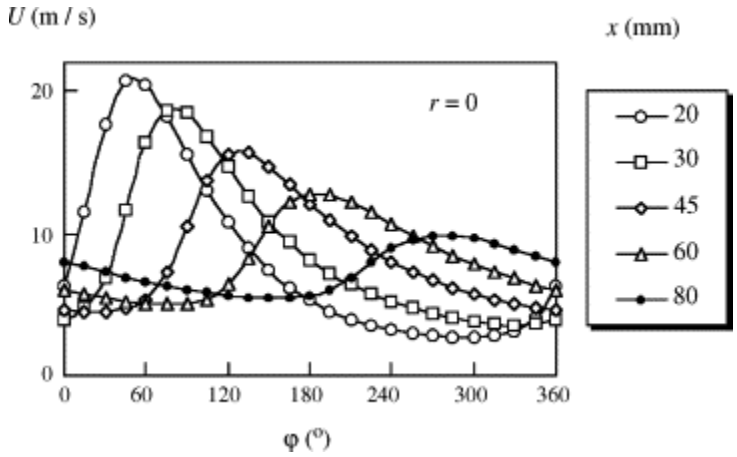

Fig. 6. Computed centerline velocity during one cycle-development of cycle shape.

The streamwise variation of the time-mean velocity along the jet centerline is shown in Fig. 7. The measured velocity development is evidently proportional to x^n, thus the exponent n was evaluated by the least squares fit as $n = -0.15$ and -1.09 for $x < 90$ mm and $x > 90$ mm, respectively. As is well known for conventional axisymmetric fully developed turbulent jets, this proportionality is $x^{-1.0}$, see for e.g., Schlichting [28]. A rapid change of slope of a conventional jet is related with the end of its potential core. A reason for a similar behavior of the present D-SyJ is, generally speaking, a different character in near and far flow field under the periodic actuation; evidently, this subject will need further investigation focusing on process of formation of the D-SyJs. It is worthy to note here that experiments by Smith and Glezer [5] with a two-dimensional zero-net-mass-flux synthetic jet gave an exponent a bit higher than of conventional jets, namely −0.58 while for conventional 2D fully developed turbulent jet this proportionality is $x^{-0.5}$.

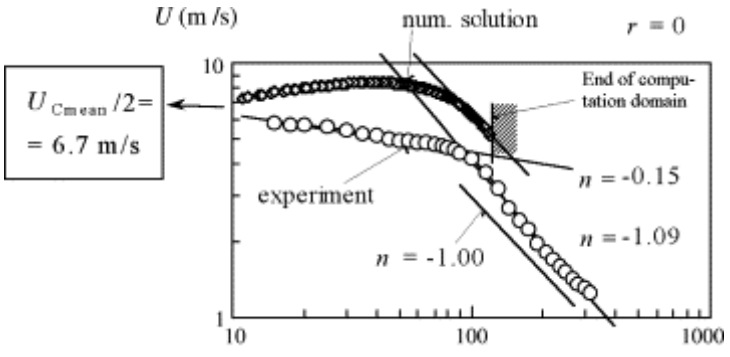

Fig. 7. Variation of the time-mean centerline velocity with axial distance.

A comparison of experiments with numerical simulations is plotted in Fig. 7 as well. A character of computed time-mean velocity decay is qualitatively similar, however, quantitative agreement is still quite far from satisfactory, numerical simulations give over-predicted values of centerline velocities.

Further, Fig. 7 shows an agreement with the velocity $U_{\mathrm{Cmean}}/2 = 6.7$ m/s, where U_{Cmean} is the time-mean velocity at the exit plane of the central nozzle during the pump stroke. The evaluation was made according to the actuation analysis [1]: the sinusoidal character of periodic operations implies $U_{\mathrm{Cmean}}/2 = U_{\mathrm{Cmax}}/\pi$, where U_{Cmax} is the maximum velocity at the exit plane; the value $U_{\mathrm{Cmax}} = 21.0$ m/s was taken from Table 2 in [1]. One half of the U_{Cmean} is considered here, because the pump stroke is assumed to be "expanded" over the whole cycle (similar approach as at the definition of the Reynolds number in Eq. (25) in [1]).

An example of velocity profiles is presented in Fig. 8. The data points are plotted in dimensionless form. The velocity values are related to the maximum value on the jet axis U_{CL}. On the horizontal co-ordinate, the actual radial distance r is divided by the distance from the axis to the point where velocity magnitude is one half of the axial velocity $r_{0.5}$. A large number of such profiles were measured at various distances from the nozzle ranging from $x = 20$ to 80 mm. The values plotted in the diagram are representative ones for large distances from the nozzle. There are several sets of data points. Some were obtained from the numerical computations at time-mean velocity profiles (evaluated as the average from 24 profiles in the cycle). Also plotted in Fig. 8 are time-mean experimental velocity values at the same distance. In this presentation, all the velocity profiles are on practically the same curve. An important finding, moreover, is that this resultant curve is identical to the velocity profile obtained by the similarity solutions of steady jets [29]: The one-equation solution [30], based upon the assumption of constant characteristic size of turbulent vortices in the jet cross section, is practically indistinguishable from the two-equation solution [31] and [32] which needs no such preliminary assumption. This is an interesting fact about radial transport of momentum in the generated jet, indicating that this takes place mainly by vortices having the same size across the whole jet cross section. In the other words a behavior of the jet for large distances from the nozzle is well comparable with the well known conventional axisymmetric fully developed turbulent jets [28].

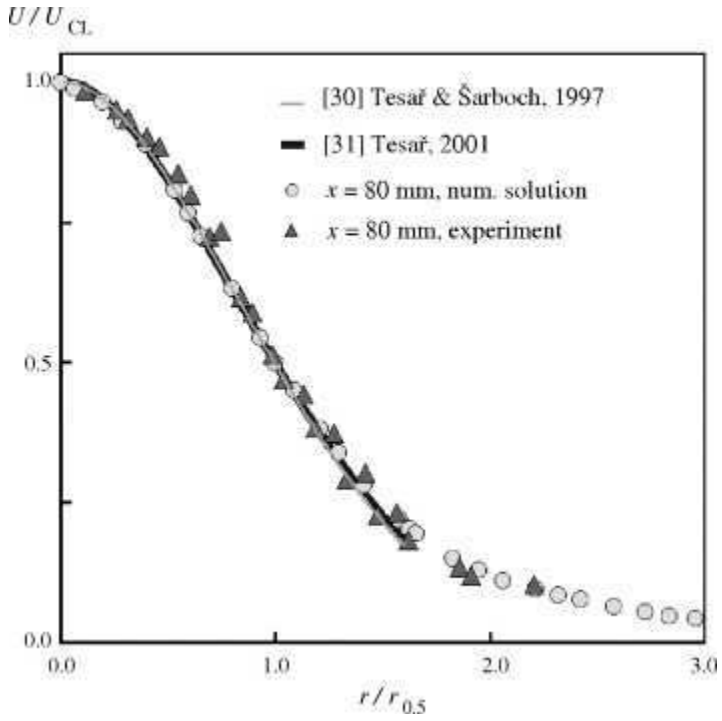

Fig. 8. Cross-stream distribution of the time-mean streamwise velocity: a comparison of experiments with numerical simulations.

6. Conclusions

Numerical and experimental studies of the performance of the new actuator for fluid jet generation have been performed. In principle, the operation of the actuator is based on the combination of synthetic jet generation and fluidic pumping by a valve-less reciprocating pump. The resulting periodical fluid jet is an intrinsically non-zero-net-mass-flux, in contrast to the traditional synthetic jet. Besides, the present actuator operates in a double-acting regime.

The presented results have confirmed the satisfactory performance of the double-acting actuator. For large distances from the nozzle, the generated jet is comparable with the well-known conventional axisymmetric fully developed turbulent jets.

The results have also proved that the CFD software used to obtain the numerical results provides a satisfactory description of the complex and periodic flowfield and can be used for further investigations.

Acknowledgments

We gratefully acknowledge the support by the Institute of Thermomechanics, Academy of Sciences of the Czech Republic (project AV0Z20760514), and by the National Science Council, Taiwan (NSC 91-2811-E-002-020). The financial support for the short visit of Prof. V. Tesař at the Institute of Applied Mechanics, National Taiwan University, provided by the Optomechatronics Education Resource Center, Ministry of Education, Taiwan, is also acknowledged.

References

[1] Z. Trávníček, A.I. Fedorchenko and A.-B. Wang, Enhancement of synthetic jets by means of an integrated valve-less fluid pump. Part I. Design of the actuator, *Sens. Actuators A* **120** (2005), pp. 232–240.

[2] A. Glezer, M.G. Allen, D.J. Coe, B.L. Smith, M.A. Trautman, J.W. Wiltse, Synthetic Jet actuators and applications thereof, US Patent no. 5,758,823, 1998.

[3] V. Tesař, Fluidic pump driven by alternating air flow, *Proceedings of PNEU-HIDRO'81 IV. Colloquium on Pneumatics and Hydraulics* Györ, Hungary (1981).

[4] V. Tesař, Fluidic jet-type rectifier: experimental study of generated output pressure, *J. Fluid Control/Fluid. Quart.* **14** (1983) (4), pp. 13–27.

[5] L. Smith and A. Glezer, The formation and evolution of synthetic jets, *Phys. Fluids* **10** (1998), pp. 2281–2297.

[6] A. Glezer and M. Amitay, Synthetic jets, *Annu. Rev. Fluid Mech.* **34** (2002), pp. 503–529.

[7] S.G. Mallinson, J.A. Reizes and G. Hong, An experimental and numerical study of synthetic jet flow, *Aeronaut. J.* **105** (2001), pp. 41–49. Abstract + References in Scopus | Cited By in Scopus

[8] B.L. Smith and G.W. Swift, A comparison between synthetic jets and continuous jets, *Exp. Fluids* **34** (2003), pp. 467–472.

[9] V. Tesař and S. Zhong, Efficiency of synthetic jets generation, *Trans. Aeronaut. Astronaut. Soc. Rep. China* **35** (2003) (1), pp. 45–53.

[10] B.L. Smith and A. Glezer, Jet vectoring using synthetic jets, *J. Fluid Mech.* **458** (2002), pp. 1–34.

[11] M. Amitay and A. Glezer, Controlled transients of flow reattachment over stalled airfoils, *Int. J. Heat Fluid Flow* **23** (2002), pp. 690–699.

[12] J. Tensi, I. Boué, F. Paillé and G. Dury, Modification of the wake behind a circular cylinder by using synthetic jets, *J. Visualiz.* **5** (2002) (1), pp. 37–44.

[13] R. Mittal and P. Rampunggoon, On the virtual aeroshaping effect of synthetic jets, *Phys. Fluids* **14** (2002), pp. 1533–1536.

[14] M. Benchiekh, J.-C. Bera, M. Michard and M. Sunyach, Pulsed jet control of a short diffuser, Mécanique des fluides/Fluids Mechanics: Series IIB, vol. 328, C.R. Acad. Sci, Paris (2000) 749–759, (in French).

[15] Z. Trávníček and V. Tesař, Annular synthetic jet used for impinging flow mass-transfer, *Int. J. Heat Mass Transfer* **46** (2003), pp. 3291–3297.

[16] Y. Yassour, J. Stricker and M. Wolfshtein, Heat transfer from a small pulsating jet, *Proceedings of the 8th International Heat Transfer Conference, vol. 3* Hemisphere Publ., San Francisco, USA (1986), pp. 1183–1186.

[17] M.B. Gillespie, Local convective heat transfer from heated flat plates using synthetic air jets,Thesis, Georgia Institute of Technology, USA (1998).

[18] S.G. Mallinson, C.Y. Kwok and J.A. Reizes, Numerical simulation of micro-fabricated zero-mass-flux-jet actuators, *Sens. Actuators A* **105** (2003), pp. 229–236.

[19] G.H. Priestman and J.R. Tippetts, Development and potential of power fluidics for process flow control, *Chem. Eng. Res. Design* **62** (1984), pp. 67–80.

[20] V. Tesař and K. Peszynski, Non-moving-part fluidic circulation pumps, Proceedings of XII ICMR colloquium, *Bydgoszcz, Poland* (2003), p. 191.

[21] E. Stemme and G. Stemme, A valve-less diffuser/nozzle-based pump, *Sen. Actuators A* **39** (1993), pp. 159–167.

[22] T. Gerlach, M. Schuenemann and H. Wurmus, A new micropump principle of the reciprocating type using pyramidic micro flow channels as passive valves, *J. Micromechan. Microeng.* **5** (1995) (2), pp. 199–201.

[23] F.K. Forster, R.L. Bardell, M.A. Afromowitz, N.R. Sharma and A. Blanchard, Design, fabrication and testing of fixed-valve micro-pumps, *Proceeding of the ASME Winter Annual Meeting, Nov. 1995, vol. 234* San Francisco.

[24] L.S. Pan, T.Y. Ng, X.H. Wu and H.P. Lee, Analysis of valveless micropumps with inertial effects, *J. Micromechan. Microeng.* **13** (2003) (3), pp. 390–399.

[25] A. Olsson, G. Stemme and E. Stemme, Numerical and experimental studies of flat-walled diffuser elements for valve-less micropumps, *Sens. Actuators A* **84** (2000), pp. 165–175.

[26] Z. Trávníček, A.I. Fedorchenko, A.-B. Wang, An enhancement of synthetic jets by means of an integrated valveless pump. in: J.J. Wijetunge (Ed.), Proceedings of the Tenth Asian Congress of Fluid Mechanics (ACFMX), May 17–21, 2004. Peradeniya, Sri Lanka, Book of Abstracts, full text is on the CD-ROM, pp.535–540.

[27] FLUENT User's Guide, Release 5.5.14. FLUENT Inc., Lebanon, 1998.

[28] H. Schlichting, Boundary Layer Theory (seventh ed.), McGraw-Hill, New York (1979).

[29] V. Tesař, Similarity solutions of basic turbulent shear flows with one- and two-equation models of turbulence, Zeitschrift für Angewandte Mathematik und Mechanik 77 (1997) 333.

[30] V. Tesař and J. Šarboch, Similarity solution of the axisymmetric turbulent jet using the one-equation model of turbulence, *Acta Polytechn. J. Adv. Eng.* **37** (1997) (3), pp. 5–34.

[31] V. Tesař, Two-equation turbulence model similarity solution of the axisymmetric fluid jet, *Acta Polytechn. J. Adv. Eng.* **41** (2001) (2), p. 26.

[32] V. Tesař, The problem of round jet spreading rate computed by two-equation turbulence model, Proceeding of Conference on Engineering Mechanics 97, Svratka, Czech Republic, May 1997, 181–186.

Authors' Profiles

Zdeněk Trávníček: He received his degree in Mechanical Engineering from the Czech Technical University (ČVUT) in Prague in 1985. From 1985 to 1995 he was employed at the former National Research Institute for Machine Design (SVÚSS) in Prague- Běchovice. He received his PhD degree from ČVUT in Prague in 1994. In 1996, he joined the Institute of Thermomechanics, Academy of Sciences of the Czech Republic. The most significant stays abroad: Institute of Engineering Thermophysics of the Ukrainian Academy of Sciences (ITTF, Dept. of Prof. J.P. Dyban), Kiev, Ukraine (1990); Institute of Applied Mechanics, National Taiwan University, Taipei, Taiwan R.O.C (1998–1999, and 2002–2003); Heat Transfer Laboratory, Johns Hopkins University, Baltimore, USA, (2000/2001). His research interests cover convective heat and mass transfer from surfaces exposed to flows, experimental fluid mechanics, influence of a (jet) flow structure on heat transfer, passive/active controls of fluid flows, forced convective heat transfer enhancement, jet flows (primarily impinging jets). He is the author of 38 research reports and 76 papers published in various journals or conference proceedings.

Václav Tesař: He received his degree in Mechanical Engineering in 1963 from the Czech Technical University (ČVUT), Prague, Czech Republic. From 1963 to 1999 he

was employed at ČVUT in Praha as Assistant, later Docent, and finally Full Professor. He recived C.Sc. degree (an equivalent of PhD) from ČVUT Praha in 1972. From 1994 to 1998 he was the Head of the Department of Fluid Mechanics and Thermodynamics, Faculty of Mechanical Engineering ČVUT Praha. In 1985 he was Visiting Professor at Keio University, Yokohama, Japan. In 1992 he stayed as Visiting Professor at Northern Illinois University, DeKalb, USA. Since 1999 is employed as Professor at the Process Fluidics Group, Department of Chemical and Process Engineering, the University of Sheffield, United Kingdom. His research interests cover fluid mechanics in general, mainly flow visualization and study of turbulence, and concentrate particularly on studies of jets and wall jets, including their applications in fluidics for non-moving-part flow control (he is named as the inventor on 195 Czech Patents, mainly concerning fluidic devices). Recently became involved in the new field of microfluidics. He is an author of four textbooks and over 270 papers in various journals and conference proceedings.

An-Bang Wang: He received the BS degree from the National Cheng-Kung University in 1979, the MS degree from the National Tsing-Hua University in 1981. After the 2-year military service, he served as a mechanical engineer, project manager and head of the mechanical department at the Sinotek Automation Company, Taipei, Taiwan from 1983 to 1985. He was then awarded the 3-year Abroad-study scholarship of the Educational Ministry, Taiwan. From 1988 to 1991, he worked as a scientific researcher at the Institute of Fluid Mechanics, University of Erlangen-Nürnberg, Germany, and received the Dr.-Ing. degree there in 1991. He joined the Institute of Applied Mechanics, National Taiwan University in 1991 and became a full professor in 2001. Since 2002, he served as the director of Optomechatronics Education Resource center, Ministry of Education, Taiwan, ROC. He is a member of many international/domestic academic societies, such as AAAS, APS, and Society of Theoretical and Applied Mechanics, ROC (life) etc. He is the author of about 150 publications in various journals, conference proceedings, reports and patents. He is also reviewer of many international/domestic academic journals and grants agencies of government. Numerous students received best paper awards in various competitions under his supervision. His current research interests include Bio-chip and micro-flow systems, optomechatronic systems, flow separation and control, and new measuring techniques.